ELSEVIER

Journal of Alloys and Compounds 275–277 (1998) 526–532

Journal of ALLOYS AND COMPOUNDS

X-ray magnetic circular dichroism as a tool for magnetic studies of 4f compounds

E. Dartyge*, F. Baudelet, C. Giorgetti, S. Odin

LURE, Université Paris Sud, 91405 Orsay Cedex, France

Abstract

A short review is given of the theoretical fundamentals, applications and limitations of X-ray magnetic circular dichroism (XMCD) at the $M_{4,5}$ and $L_{2,3}$ edges of rare earth compounds. © 1998 Elsevier Science S.A.

Keywords: X-ray magnetic circular dichroism; $M_{4,5}$; $L_{2,3}$; Rare earth

1. Introduction

Dichroism is the property of a sample to absorb or emit with different cross-section photon beams with different polarization. Linear dichroism is for two mutually perpendicular polarizations of light, circular dichroism (which is the subject of the paper) concerns the difference of absorption between right and left polarized photons. This difference is due to the breaking of spherical symmetry of the absorbing atoms: it may be a structural anisotropy of the electronic density of the material and, in that case, the dichroism is *natural* or it may be a magnetic anisotropy (for ferro- or ferrimagnetic compounds) and the dichroism is *magnetic* (XMCD). These magneto optic effects are well known in the visible range of energies as the Faraday effect for transmission experiments and the magneto optic Kerr effect in reflection mode (MOKE). The physics are the same in the X and visible range of energies, the interaction of the photons with the absorbing atoms can be treated in the frame of the electric dipole approximation (E_1) and in some cases in the quadrupole approximation (E_2). However, because of the different energies of the photons, the Faraday effect or MOKE concern transitions of the photoelectron from the occupied to the empty states of the valence band, whereas in the X-ray case, the photoelectron is excited from a well-defined atomic core level into the vacant valence states. In principle the theoretical interpretation of the data should be easier in this last case. Another advantage is that non-transparent to visible light bulk materials such as metals can easily be studied.

The interaction Hamiltonian is mainly the electric dipolar operator, which only acts on space variables so the spin moment of the atom is only indirectly involved in the transition of the photoelectron by the spin orbit interaction. So, to observe XMCD, it is necessary to satisfy three conditions: the photons must be circularly polarized, the material must possess a magnetic moment, and the spin orbit interaction must be present. The first condition was not easily fulfilled before the advent of synchrotron sources and it is the reason why XMCD has developed only during the last 10 years. It appears as a powerful tool thanks to the adjustable wavelength, and the restrictive selection rules which allow the orbital selectivity of the probed final states and an atomic selectivity of the excited atom by choosing a specific edge.

For rare earth compounds the $M_{4,5}$ ($3d_{3/2,5/2} \rightarrow 4f_{5/2,7/2}$ transitions) and $L_{2,3}$ ($2p_{1/2,3/2} \rightarrow 5d_{3/2,5/2}$ transitions) edges are the most studied. These edges are split by the spin-orbit coupling acting on the core hole. They allow to probe the 4f and 5d shells of the rare earth atom. The simplest experiment is to measure two absorption spectra (σ^{-1} and σ^{1}) at a specific edge with, respectively, right and left circular polarization of light and to calculate their difference $\Delta\sigma = \sigma^{-1} - \sigma^{1}$, normalized by the isotropic absorption. The macroscopic magnetic moment of the sample must have a non-zero component parallel to the wave vector of the photons. Instead of changing the polarization of the light, it is often easier to inverse the sign of the magnetic polarization by inverting the sense of the mag-

*Corresponding author.

0925-8388/98/$19.00
PII: S0925-8388(98)00384-3

netic field which polarizes the sample. For a review of the different ways of measuring the XMCD see Ref. [1].

2. Theoretical backgrounds

The basic process is the absorption of a photon of polarization vector $\hat{\mathbf{e}}$ and the excitation of a selected atom from an initial state $|i\rangle$ into a final state $|f\rangle$. In the framework of electric dipole approximation (E_1) the cross-section for X-ray absorption is given by the golden rule:

$$\sigma(\hat{\boldsymbol{e}}) = 4\pi^2\alpha_0\hbar\omega\sum\nolimits_f |\langle f|\hat{\boldsymbol{e}}\cdot\boldsymbol{r}|i\rangle|^2\delta(E_f - E_i - h\omega)$$

where $E_f - E_i$ is the difference of energy between the final and initial states, $h\omega$ the energy of the photon, and $\hat{\mathbf{e}}\cdot\mathbf{r}$ is the electric dipolar operator. The E_1 selection rules for the transition will be given below. For simplification they will be considered transitions from a pure initial configuration to a pure final configuration without mixing of configurations in the initial or final states. The squared matrix elements of the electric dipole operator are separated in a radial part and an angular part. Depending on the nature of the final states, two models can be developed. In the case of the $M_{4,5}$ edges a 3d electron is transferred into a localized atomic-like 4f state, an atomic calculation is possible and the final state is built by coupling all the empty shells, including the core hole shell (multiplet theory). In the case of the $L_{2,3}$ edges where a 2p electron is excited into a non-localized nearly empty d band (the 2p→6s transition, which has a small cross-section, is not considered) and it is generally assumed that a one-electron approximation is valid, the influence of the core hole is neglected.

2.1. Multiplet theory

Fig. 1 (from Ref. [2]) shows the energy diagram of the allowed E_1 transitions in the case of Yb^{3+} at $M_{4,5}$ edges.

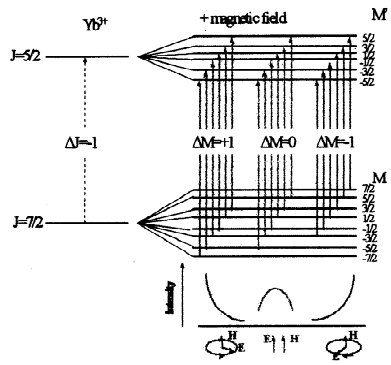

Fig. 1. Energy diagram of the $3d^{10}4f^{13}\rightarrow 3d^{9}4f^{14}$ transition of Y_b^{3+} without and with a magnetic field; The vertical arrows indicate the electric dipole allowed transitions; their relative intensity are given in Ref. [2].

J,J' and M,M' are the total angular and magnetic momentum of the atom in the initial and final states. ΔJ, ΔM are the differences between the initial and final quantum numbers. The E_1 selection rules are $\Delta J = \pm 1.0 \Delta M = 1$ (positive helicity, left polarization), $\Delta M = -1$ (negative helicity, right polarization), $\Delta M = 0$ (linear polarization). One sees in Fig. 1 that the transitions are from an initial multiplet $4f^n$ split by the Zeeman effect to the final multiplet $3d^9 4f^{n+1}$. The dichroism is due to the different ΔM selection rule for the different polarization of light. The shape and amplitude of the experimental spectra are perfectly reproduced by these multiplet calculations. The amplitude of the spectra is proportional to $\langle M\rangle$, the mean value of the projection of the magnetic moment of the ion on the quantization axis.

2.2. One-electron approximation

It is considered that only one electron is involved in the transition, the other electrons of the atom being spectators. The occupied and vacant states are calculated within a one-electron model. j,j' and m,m' are the angular and magnetic momentum of the shell in the initial and final states, Δj, Δm are the differences between their initial and final values. In this one-electron description the selection rules become $\Delta j = \pm 1$, $\Delta m = +1$ (positive helicity, left polarization), $\Delta m = -1$ (negative helicity, right polarization), $\Delta m = 0$ (linear polarization); the core hole is taken into account by allowing a kind of 'relaxation' of the final states. The simplest relaxation is described by the $Z+1$ approximation: because of the core hole the valence electrons see an effective nucleus with $Z+1$ nuclear charges. Fig. 2 gives a scheme of the mechanism of the transition which is a two-stage mechanism: because of the spin orbit coupling, circularly polarized photons excite with different probabilities up and down electrons; this leads to spin polarized photoelectrons. This spin polarization P_e is opposite for right and left polarized photons. Because $\hat{\mathbf{e}}\cdot\mathbf{r}$ does not act on the spin, this spin-polarized electron goes to one of the vacant states corresponding to its polarization; when there exists a difference between the up and down 5d band, there will be a difference in the absorption cross-section for right and left polarization.

In their pioneering work, Schütz and co-workers [3] proposed a simple law for the XMCD:

$$\Delta\sigma/2\sigma = P_c P_e \Delta\rho/\rho.$$

with σ isotropic absorption cross-section, P_e rate of spin polarization of the photoelectron, P_c rate of circular polarization of the light, and $\Delta\rho/\rho$ relative spin polarization of the final states. P_e is calculated from the Fano [4] calculation. P_e is evaluated to -0.5 for the L_2 edge and to $+0.25$ for the L_3 edge; in this evaluation one supposes that the radial matrix elements of the transition are orbital and spin independent and that only the angular part of the

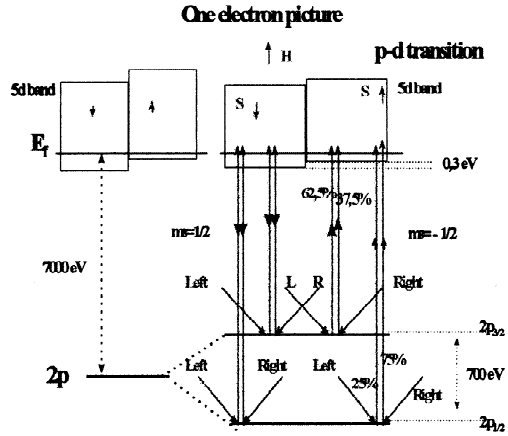

Fig. 2. Schematic diagram of the transition at L_2 and L_3 edges in the one-electron model. The initial state (left side) show the non-split 2p level and the Fermi level with a 5d band nearly empty but with an exchange splitting between the minority and majority sub-bands. The absorption of a photon excites a 2p electron to an empty state of the band of the same spin moment; the core hole split the 2p level in two $2p_{1/2}$ (L_2) and $2p_{3/2}$ (L_3) levels (right side). The probability of photo-excitation of the electron is calculated taking all the possible p–d transition matrix elements at the two edges (Clebsch–Gordan calculations for the two polarization of light); the results are shown only for the minority spins. In this calculation, the spin orbit in the 5d band is neglected. The magnitude of the energy splitting and the position of the Fermi level are typical of rare earth but may change from a sample to an other. In ionic compounds, the 5d band is empty.

matrix elements are different. It will be shown that this description does not work for the $L_{2,3}$ edges of the rare earth with a 4f moment; it is applicable to compounds with no 4f moments, that means compounds with La, Lu, or mixed valent Ce. In these last cases, it is possible to evaluate the moment of the d band, which is a moment induced by the magnetic neighbors of the rare earth. An important consequence is that the applicability of this simple law will be a sensitive test of the valence state of the cerium compounds.

2.3. Sum rules

The first sum rules in X-ray absorption spectroscopy have been developed by Thole and van der Laan [5] who studied the branching ratio B of $M_{4,5}$ and $L_{2,3}$ edges: $B=I(M_5)/(I(M_5)+I(M_4))$ or $I(L_3)/(I(L_3)+I(L_2))$. They showed that $B=B^0+A\langle i|Z|i\rangle$ where Z is the angular part of the spin-orbit operator in the initial state $|i\rangle$, A is a proportionality constant which depends on h, number of holes per atom: $A=-1/3h$ for L edges and $A=-4/15h$ for M edges. B^0 is equal to the statistical value when the electrostatic interaction core-valence is negligible, and in other cases B^0 depends on the value of the core-valence Slater integrals. Thole et al. [6] and Carra et al. [7] found magnetic sum rules for XMCD which allow to separate the spin and orbital contribution to the magnetic moment of the atom.

2.3.1. Orbital sum rules

For a transition between a core level c to a valence level l with n electrons in the ground state, and neglecting the $l=c-1$ channel the orbital sum rule is:

$$\frac{\int_{J^+ + J^-}(I^{-1}-I^1)}{\int_{J^+ + J^-}(I^1+I^0+I^{-1})}=\frac{-\langle 0|Lz|0\rangle}{lh}$$

where h is the number of holes in the l shell: $h=4l+2-n$; I is the normalized polarized absorption cross-section,

$$I^q=\frac{1}{4\pi^2\alpha\hbar\bar{\omega}}\sigma^q(\bar{\omega})$$

with $q=1$ for left polarized photons, -1 for right polarized photons and 0 for linear polarization parallel to the magnetic polarization. $\langle L_z\rangle$ is the mean value of the z component of the orbital momentum operator L (z is along the quantization axis). The integral over J^+ and J^- is over the $J=c+1/2$ and $J=c-1/2$ edges energy range. When the orbital moment is zero, the integral is zero, which gives a ratio -2 between the XMCD normalized at L_2 and L_3 edges (or -1 without normalization). The opposite sign of XMCD at the L_2 and L_3 edges comes from the opposite spin-orbit coupling of the core states.

These sum rules have been applied with success to the $M_{4,5}$ edges of rare earths but fail at the $L_{2,3}$ edges of rare earth compounds with 4f moments, where it leads to unphysical results. They suppose the validity of two strong approximations: the energy and spin independence of the radial matrix elements of the transition; this statement is probably not justified for L edges, because of the large energy range of the integration domain, and because of the strong 4f–5d exchange which may modify differently the spatial wave functions of the up and down 5d band [8]. In this last case, there is another limitation due to the eventual contribution of quadrupolar transitions with final 4f shell states; in the case of absorption this contribution has a very small cross-section when compared to the dipolar one, but its effect on dichroism may be important, because the magnetic 4f moment is much greater than the 5d one. This may lead to erroneous evaluation of the integrals.

2.3.2. Spin sum rule

Considering again only the $l=c+1$ channel and with the same notation, the spin sum rules are:

$$\frac{\int_{J^+}(I^{-1}-I^1)-\frac{l}{l-1}\int_{J^-}(I^{-1}-I^1)}{\int_{J^+ + J^-}(I^1+I^0+I^{-1})}=\frac{-2}{3h}(\langle 0|S_z|0\rangle+\frac{2l+3}{l}\langle 0|T_z|0\rangle)$$

$\langle S_z\rangle$ is the ground state average value of the z component of the spin operator S and $\langle T_z\rangle$ of the magnetic dipole

operator T taken on the l shell. $\langle T_z \rangle$ describes any correlation between the spin and position of each electron in the shell. The validity conditions are the same as for the orbital sum rules with, in addition, the necessity of a sufficient energy gap between the J^+ and J^- edges in order to avoid any overlapping. This last condition has to be carefully verified for the $M_{4,5}$ edges. Another problem is the evaluation of $\langle T_z \rangle$. In the case of a pure J state $\langle T_z \rangle$ can be calculated; this is generally the case for the $M_{4,5}$ edges of the rare earth compounds with well-localized 4f electrons. The number of holes must also be known; however, when $\langle T_z \rangle$ may be neglected, one can evaluate the ratio $\langle S_z \rangle / \langle L_z \rangle$, eliminating h and the normalization problems.

In summary, the sum rules are mainly used at the $M_{4,5}$ of the rare earths for measuring $\langle L_z \rangle$ and $\langle S_z \rangle$ of the 4f shell and, in some cases, at the $L_{2,3}$ edges for mixed valent cerium compounds where the 4f electron is hybridized with the conduction band or for La and Lu compounds because they are without 4f moment.

3. Application to rare earth magnets

The first experiments performed on rare earth compounds aimed at verify the validity of the theoretical predictions for XMCD; accordingly the measurements were done on magnetically well-characterized samples. This is still the case for the L edges which resist a complete understanding of the relevant parameters. In the case of the $M_{4,5}$ edges the multiplet calculations are so accurate that it is possible to use them to characterize the 4f magnetic state of compounds where the spin-resolved band structure is unknown.

3.1. $M_{4,5}$ edges

The multiplet calculation for the $M_{4,5}$ absorption edges of the whole set of rare earth atoms was published in 1989 by Goedkoop [2]. Cowan's program [9] was used, with a reduction of the Hartree–Fock values for the Slater integrals in order to take into account the solid effects. The different authors who worked on this spectroscopy performed the same kind of calculations, and in addition employed the sum rules. The theoretical spectra agree fairly well in shape with the experimental ones. Some examples of what can be obtained are given:

Suga and Imada [10] studied a dense Kondo material, Sm_4As_4 showing a ferromagnetic transition at 160 K. They performed the $M_{4,5}$ and $N_{4,5}$ XMCD at the Sm edges; the shape of the spectra agree with atomic calculations of a Sm^{3+} ion. However, the sign of the XMCD at each edge is opposite to the theoretical calculations. From these observations they conclude that, in Sm^{3+}, the total 4f magnetic moment $\mu = -\mu_b(L+2S)$ is aligned with the field. L and S are antiparallel and nearly compensate, and that the sign of the XMCD indicates that $2S$ is the leading term in this material. The authors used the L_z and S_z sum rule neglecting T_z. They obtained a ratio $L_z/S_z = 1.95$ for the 4f shell which confirms the dominating role of $2S_z$ and explains the opposite sign of the dichroism. In contrary, in the permanent magnet $Nd_2Fe_{14}B$, the 4f shell of Nd^{3+} has the same antiparallel situation of L and S but it is L which dominates. The Nd and Fe moments are parallel and oriented along the macroscopic moment with the 3d and 4f spins antiparallel. In this last case, the $M_{4,5}$ XMCD agree in shape and sign with the atomic calculations (note that XMCD at the $L_{2,3}$ edge of Fe was also studied, providing a separate evaluation of the 3d and 4f shells).

XMCD at Er $M_{4,5}$ [11] was used to follow the H,T magnetic phase diagram of an amorphous Er_{27}–Fe_{73} alloy. In these samples, macroscopic measurements of the magnetic moment show a strong evolution of the compensation temperature with the applied magnetic field. The variation of XMCD at Er $M_{4,5}$ is consistent with a magnetic fan structure of both the Er and Fe atoms. It shows the existence of temperature-induced, as well as field-induced, flips of the Er sub-lattice with respect to the direction of the magnetic field, evidenced by the change of sign of the dichroism.

XMCD is also effective in the study of 5f materials. The energy domain of the spectroscopy (3 keV) was not so easily accessible as for the 4f elements, but the new synchrotron sources have allowed the experiments since a few years ago. The first experiments [12] on one US crystal have revealed important differences with the 4f compounds: due to the strong spin-orbit interaction in the 5f shell, the spin sum rules must be applied without neglecting $\langle T_z \rangle$ which is often more important than $\langle S_z \rangle$. $\langle T_z \rangle$ is calculated in the framework of intermediate coupling. XMCD is better reproduced with atomic calculation for $5f^2$ and $5f^3$ mixing than with a pure Hund's rule ground state. In UFe_2 [13] where the 5f electrons are itinerant, the branching ratio of the U $M_{4,5}$ edges is interpreted with a number of 5f electrons nearly equal to 2, and the XMCD is consistent with an 5f orbital moment parallel to the total magnetic moment, a quasi-total cancellation between the spin and orbital moment, in agreement with the polarized neutron experiments. Grange et al. (this conference) measured XMCD in URhAl which is a ferromagnet below 27 K and compared the spectra with those of UFe_2 (itinerant magnetism) and $USb_{0.5}Te_{0.5}$ (localized magnetism). They show that the state of localization of the 5f wave function of URhAl is intermediate between these last two materials.

XMCD has been widely used to characterize mixed valent cerium materials combining M and L edges studies. A separate section will be devoted to this special case.

3.2. L edges

Systematic studies have been performed on several series of rare earth transition metal (TM) intermetallic crystals, amorphous materials and insulating ferromagnetic

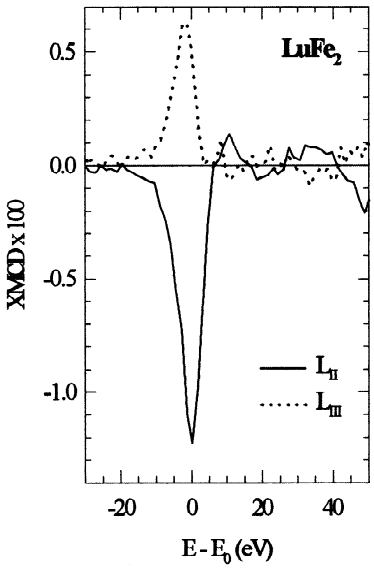

Fig. 3. Normalized XMCD at L_2 and L_3 edges of Lu for $LuFe_2$. Note the −2 factor between XMCD at the two edges. This factor should be −1 for the non-normalized spectra of the same sample, yielding to a zero integrated XMCD. The origin of energies is taken at the inflection point of the absorption edge.

oxides in order to extract the relevant physical effects which govern the XMCD of L edges [14].

Figs. 3 and 4 show the XMCD for the series of the available Laves phase rare earth Fe_2, giving an example of what is understood and what remains to be solved. For Pr and Nd atoms the rare earth Fe_2 compounds are synthesized with difficulty, so the spectra of $PrCo_2$ and Nd_2Fe_{17} are presented in order to show that they have a similar behavior as $SmFe_2$.

3.2.1. Firstly, what is understood

$LuFe_2$ has no 4f moment because of its $4f^{14}$ shell. However, Lu atoms bear a 5d magnetic moment because of the hybridization of the 5d band with the Fe 3d band. The coupling of the 3d–5d spins is antiparallel because of the less than half filled 5d shell and the more than half-filled 3d shell [15]. This results in a positive dichroism at L_3 and negative at L_2, as observed in Fig. 3 in the case of $LuFe_2$. There is no 5d orbital moment so the integrated XMCD over the two edges is zero, in agreement with the orbital sum rules. This is also verified for La and Hf intermetallics, for the mixed valent Ce compounds and more generally for compounds with zero or nearly zero 4f orbital moment. In these cases it is possible to deduce the 5d spin moment which is proportional to the integrated area at one edge.

3.2.2. Secondly, what remains to understand

Looking at the other spectra in Fig. 4, one can see that the shape and even the sign of the XMCD are in contradiction with the simple rule previously given. The 5d band in the whole 4f series of Laves phases should not change dramatically from one rare earth to another: the

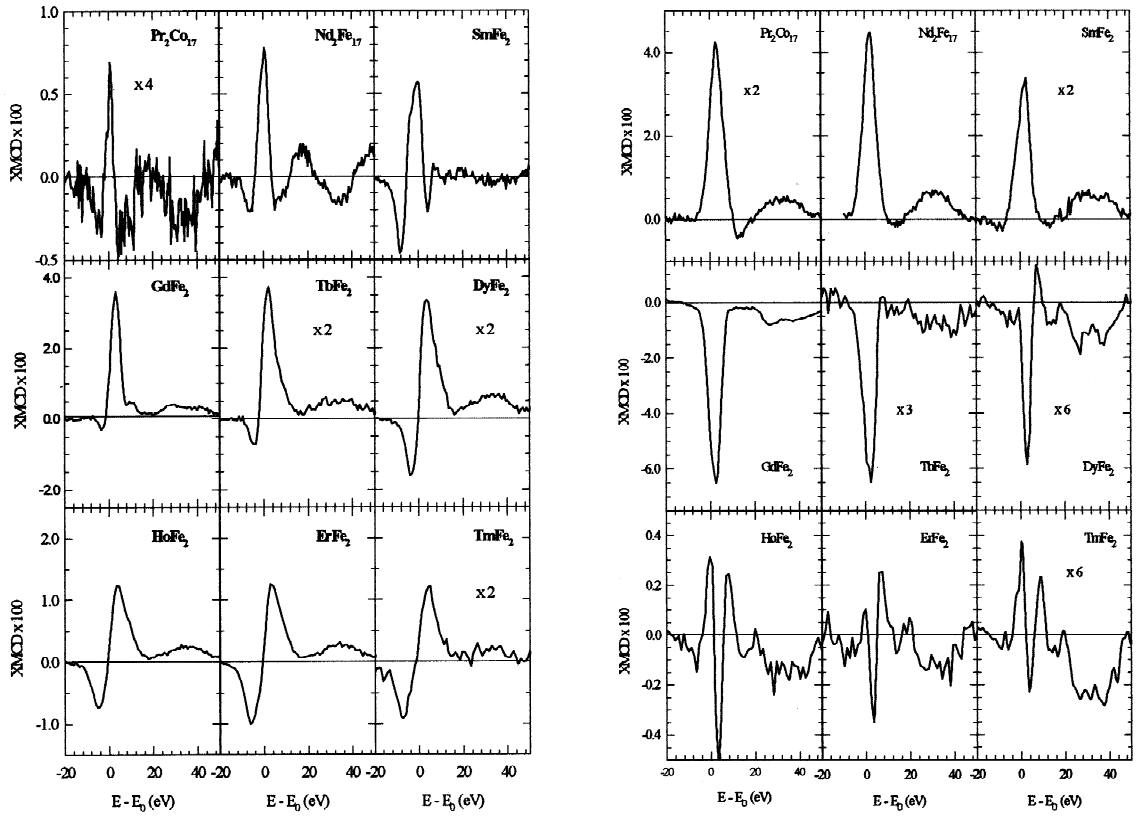

Fig. 4. Normalized XMCD of rare earth compounds: (a) L_3 edge, (b) L_2 edge. Origin of energies at the inflection point of absorption.

spins of the 5d band are antiparallel to the 3d ones, and the sign of the dichroism should reflect the sign of the 5d spin moment in respect with the sense of the bulk magnetic moment of the sample. A change of sign of XMCD is expected when passing from the light to the heavy rare earth because of the change of spin orbit coupling $L-S$ to $L+S$ in the 4f shell, following Hund's rule, and the strong intra-atomic coupling which aligns the 4f and 5d spins, but except that fact no large difference should be observed between the different spectra. Because no important 5d orbital moment is expected in this non-localized d band, the orbital sum rules predict and a zero integrated value of XMCD and an opposite sign for the XMCD at L_2 and L_3. None of these predictions is observed and there exist strong variations from one rare earth to another and between L_2 and L_3 (see Fig. 4a and Fig. 4b). This shows that the theory must be improved. It seems that the full 4f–5d Coulomb exchange interaction has to be taken into account in the calculations. Nevertheless, a qualitative utilization of XMCD has been done in measuring the variation of the amplitude of the XMCD of rare earth/transition metal multilayers with the thickness of the layers [16].

4. The case of cerium

The problem addressed here is the special comportment of the 4f electron which is at the borderline between localized and itinerant situations; in addition, the role of the 5d electrons strongly coupled with the 4f in the localized compounds is not clear in the non-localized Ce. XMCD is very sensitive to the valent state of Ce:

The most striking variation is for Ce compounds when Ce changes from mixed valent to Ce^{3+}. One can see in Fig. 5 the XMCD of $CeFe_2$ (mixed valent), and $CeRu_2Ge_2$ (trivalent), with their absorption spectra at L_2 edge. The dichroism changes of shape, sign and amplitude between the two compounds. The $CeRu_2Ge_2$ presents a XMCD analogous to the other trivalent ions such as Pr^{3+}, on the contrary in $CeFe_2$ the sign of XMCD is analogous to that of $LuFe_2$. Furthermore, the XMCD of $CeFe_2$ at L_2 and L_3 edges present the statistical ratio -2 leading to a zero orbital moment. This sensitivity of the shape of XMCD has been used by many authors to characterize the valence state of Ce in a great variety of Ce compounds. In the case of Ce–Fe compounds, the comparison of the isotropic absorption and the XMCD allows one to follow the variation of both the valence state and the 5d moment. In addition the comparison of XMCD at the M and L edges gives a separate evaluation of the 5d and 4f moment.

Isnard et al. [17] compared XMCD and absorption in the coercive $Ce_2Fe_{17}H_y$ and $Ce_2Fe_{17-x}Ga_xH_y$ compounds at the $L_{2,3}$ edges. They show that Fe to Ga substitution or hydrogen insertion have similar effects, they lead to significant re-localization of the 4f state of cerium, and that their effect are additive; however, no strong localized 4f moment (absence of α to γ transition) is observed and the 5d magnetic moment is of pure spin origin (no orbital contribution). This moment is antiparallel to the moment of

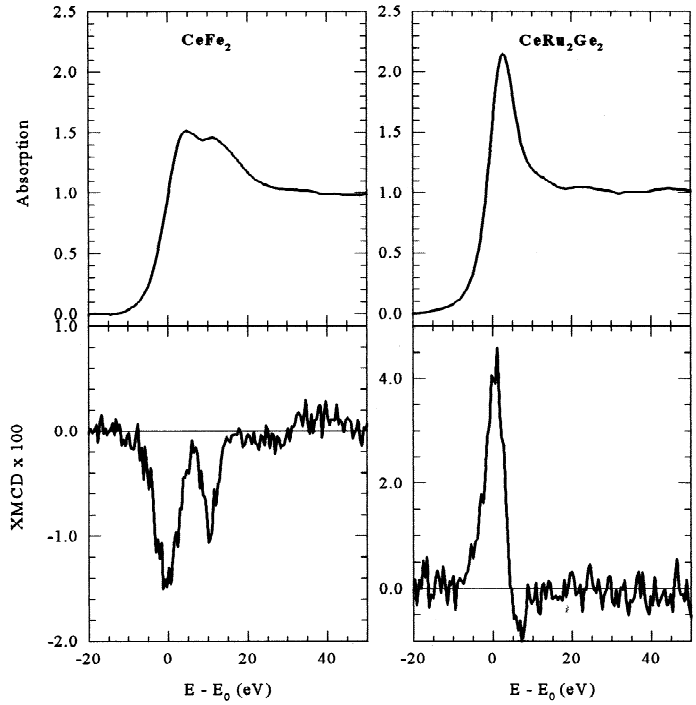

Fig. 5. Normalized absorption (top) and XMCD (bottom) of $CeFe_2$ and $CeRu_2Ge_2$ at L_2edge, measured at 4.2 K. Origin of energies at the inflection point of absorption.

Fe and is induced by the Fe atoms. The question which arises is how the 4f moment interacts with these 5d and 3d moments.

This question has been extensively studied by comparing the $M_{4,5}$ and $L_{2,3}$ XMCD for compounds where Ce is trivalent (γ) and Ce/Fe multilayers where the Ce is mixed valent (α) [18]. It shows that the M absorption and XMCD of the αCe are interpreted as resulting from a ground state described by a combination of $4f^0L$ (L represents an electron in the conduction band), $4f^1_{J=5/2}$, $4f^1_{J=7/2}$, and the γCe by a $4f^1_{J=5/2}$ only. The crystal field parameter is smaller than the spin orbit separation in γCe, but in αCe the delocalization of the 4f electron reduces the separation of the $J=5/2$ and $J=7/2$ levels and increases the crystal field effects; the 4f spin moment is parallel to the 5d one and antiparallel to the Fe moment Because of the mixing of J, a complete treatment of the spectra is not possible, but qualitative arguments allow the authors to calculate the relative weight of the $J=5/2$ and $J=7/2$ terms between 0.10 and 0.15.

Inserting a 5-Å La layer between the Fe and Ce layers suppresses the 4f moment, but not the 5d moment which persists even for a 20-Å La interlayer [18]; a 5d moment is also observed in the La layer. The same kind of observation is made for amorphous Ce–Fe alloys with αCe concentrations ranging from 19 to 34%: XMCD at the $M_{4,5}$ edges is observed for Ce concentrations inferior or equal to 27% and disappear for the higher Ce concentrations, in opposition to the XMCD at $L_{2,3}$ edges, which is present at every concentration. The 5d–3d hybridization responsible of the 5d polarization is spatially extended, but the 4f–3d coupling needs the neighboring of Fe atoms. The strong intra-atomic 4f–5d coupling seems completely absent in these compounds where a 5d moment can be observed in the absence of a 4f one. These examples show how a magnetic Ce compound can be characterized by the complementary studies of absorption and XMCD at the $M_{4,5}$ and $L_{2,3}$ edges. Many intermediate situations may exist between these extreme cases, and it is possible to well define their 4f and 5d electronic and magnetic structures.

5. Conclusion

XMCD is now a good tool to characterize the 4f magnetic moment of rare earth compounds, and the use of the sum rules allows one to calculate the 4f L_z/S_z ratio. The 5d moment of αCe, La and Lu are also measurable by XMCD at the $L_{2,3}$ edges, and the XMCD is very sensitive to the valent state of the Ce. For the other rare earth, the theory of the XMCD at the $L_{2,3}$ needs to be improved, but can be qualitatively used to detect the 5d magnetism.

References

[1] E. Beaurepaire et al. (Eds.), Magnetism and Synchrotron Radiation, Mittelwihr School 1996, Les Editions de Physique, France, p. 19.
[2] J. Goedkoop, Thesis, Nimegue, 1989.
[3] G. Schütz, W. Wagner, W. Wilhem, P. Kienle, R. Zeller, R. Frahm, G. Materlik, Phys. Rev. Lett. 58 (1987) 737.
[4] U. Fano, Phys. Rev. 178 (1969) 131.
[5] B.T. Thole, G. Van der Laan, Phys. Rev. A38 (1988) 1943.
[6] B.T. Thole, P. Carra, F. Sette, G. Van der Laan, Phys. Rev. Lett. 68 (1992) 1943.
[7] P. Carra, B.T. Thole, M. Altarelli, X.D. Wang, Phys. Rev. Lett. 70 (1993) 694.
[8] X. Wang, T.C. Leung, B.N. Harmon, P. Carra, Phys. Rev. B47 (1993) 9087.
[9] R.D. Cowan, The Theory of Atomic Spectra, University of California Press, Berkeley, 1981.
[10] S. Suga, S. Imada, J. Electron Spectrosc. Rel. Phenomena 78 (1996) 231.
[11] L.M. Garcia, S. Pizzini, J.P. Rueff, J. Vogel, R.M. Galera, A. Fontaine, J.P. Kappler, G. Krill, J. Goedkoop, J. Appl. Phys. 79 (1996) 6497.
[12] S.P. Collins, D. Laundy, C.C. Trang, G. Van der Laan, J. Phys. C. 7 (1995) 9325.
[13] M. Finazzi, Ph. Sainctavit, A.M. Dias, J.P. Kappler, G. Krill, J.P. Sanchez, P. Dalmas de Réotier, A. Yaouanc, A. Rogalev, J Goulon, Phys. Rev. B55 (1997) 3010.
[14] Ch. Giorgetti, Thesis, Orsay, 1994; Ch. Giorgetti, S. Pizzini, E. Dartyge, A. Fontaine, F. Baudelet, C.H. Brouder, P.H. Bauer, G. Krill, S. Miraglia, D. Fruchart, J.P. Kappler, Phys. Rev. B48 (1993) 12732.
[15] I.A. Campbell, J. Phys. F Metal Physics 2 (1972).
[16] F. Baudelet, E. Dartyge, G. Krill, J.P. Kappler, Ch. Brouder, M. Piecuch, A. Fontaine, Phys. Rev. B43 (1991) 5857.
[17] O. Isnard, S. Miraglia, Ch. Giorgetti, E. Dartyge, G. Krill, D. Fruchart, J. Alloys Compounds (1998) (in press).
[18] M. Finazzi, F.M.F. de Groot, A.M. Dias, B. Kierren, F. Bertran, Ph. Sainctavit, J.P. Kappler, O. Schulte, W. Felsch, G. Krill, Phys. Rev. Lett. 75 (1995) 4654.